

Mass spectrometric and first principles study of Al_nC^- clusters

Jijun Zhao ^{a*}, Bingchen Liu ^{b,c}, Huajin Zhai ^{b,c}, Rufang Zhou ^{b,c}, Guoquan Ni ^{b,c}, Zhizhan Xu ^b

^a Department of Physics and Astronomy, University of North Carolina at Chapel Hill, Chapel Hill, North Carolina 27599-3255

^b Laboratory for Quantum Optics, ^c: Laboratory for High Intensity Optics, Shanghai Institute of Optics and Fine Mechanics, Chinese Academy of Sciences, Shanghai 201800, P.R.China

We study the carbon-dope aluminum clusters by using time-of-flight mass spectrum experiments and *ab initio* calculations. Mass abundance distributions are obtained for anionic aluminum and aluminum-carbon mixed clusters. Besides the well-known magic aluminum clusters such as Al_{13}^- and Al_{23}^- , Al_7C^- cluster is found to be particularly stable among those Al_nC^- clusters. Density functional calculations are performed to determine the ground state structures of Al_nC^- clusters. Our results show that the Al_7C^- is a magic cluster with extremely high stability, which might serve as building block of the cluster-assembled materials.

36.40.Mr, 36.40.Qv, 61.46.+w

In recent years, clusters and cluster-based materials have been a field of intensive research due to both fundamental and technological importance¹⁻⁷. The structural, electronic, magnetic, and optical properties of the clusters are different from those of constitute atoms or bulk phase and depend sensitively on the size and composition of the cluster¹⁻³. It is desirable to assemble the cluster-based materials from properly designed clusters so that the unique properties of these individual clusters can be retained^{6,7}. To be a building block of cluster-assembled materials, the cluster should be highly stable and relatively unreactive. Thus, the clusters would interact weakly with each other and maintain their identities when they are brought together in the cluster-assembled solids. A well-known example is the C_{60} solids⁸. Besides C_{60} , it has also been suggested that the metal clusters with electronic and geometric shell structure can be used to construct cluster-assembled materials⁶. In this direction, some previous theoretical efforts have been devoted to aluminum-based clusters^{6,7,9-13}. First principles calculations predicted that doping in the aluminum clusters can enhance the stability of certain magic clusters like Al_{13} and modify the physical and chemical properties of the clusters^{9,11}. The stability and electronic properties of Al_{13}K solid has also been calculated¹⁰.

Experimentally, particular attention has been paid to pure and carbon-doped aluminum clusters. The mass spectra of pure and doped Al_n clusters have been obtained by different groups¹⁴⁻¹⁷. L.S.Wang et al. have performed a combined photoelectron spectroscopy and *ab initio* study on the small neutral and anionic aluminum-carbon clusters Al_nC^- ($n = 3 - 5$)¹⁸⁻²⁰. The reaction of Al_nC^- clusters with oxygen was examined by Castleman's group and Al_7C^- was found as a magic cluster²¹.

In this work, we shall investigate the structure and stability of Al_nC^- clusters via a combination of experimental cluster mass spectroscopy and *ab initio* calculations.

Our experimental apparatus consists of a standard Smalley-type laser vaporization/molecular beam cluster source, and a Wiley-McLaren time-of-flight mass spectrometer (TOF MS)²². We use a Q-switched frequency doubled Nd: YAG laser [532nm, 15ns full width at half maximum (FWHM)] to vaporize the 6 mm graphite target rod. The aluminum target contains a trace amount of carbon with C/Al ratio as 3×10^{-4} . The laser spot on the target is less than 1 mm and the typical laser output is about 40 mJ. Pulsed He carrier gas stream (purity: 99.995%) generated from a pulsed valve is used to cool down the plasma above the target that has been produced during the laser vaporization process. The clusters synthesized in the nozzle channel will then be carried into vacuum via supersonic expansion. The high pressure of the He carrier gas is necessary for generating the anionic Al_n^- and Al_nC^- clusters in a mass range from $n = 3$ through $n = 38$. The clusters form a cluster beam after passing a skimmer (2 mm, Beam Dynamics) located about 2 cm downstream from the nozzle exit.

The cluster mass abundance distribution is analyzed by the Wiley-McLaren TOF MS driven with a negative high voltage pulse generator (EG & G Model 1211, 100 ns rise time, -2 kV voltage). The extraction and acceleration regions of the TOF MS are 2 cm and 1 cm long respectively. The length of the free-drift tube in the TOF MS is 105 cm. An X-deflector is applied immediately after the acceleration region to compensate the transverse energy of the ionized clusters. By adjusting the voltage exerted on the X-deflector, clusters in different mass ranges can be recorded. The clusters are detected by a dual-microchannel plate (DMCP) and the signal from the DMCP detector is fed into a LeCroy 9350AL digital oscilloscope (500 MHz bandwidth, 1GHz sampling rate and $2 \times 2\text{M}$ maximum record length). Typically, each mass spectrum is obtained by averaging 200 shots or more in our experiments.

In this work, all electron density functional calculations on Al_nC^- ($n=1-13$) cluster anions have been performed by using the DMol program²³. A double numerical basis including *d*-polarization function (DND) are chosen. The density functional is treated by the generalized gradient approximation (GGA) with exchange-correlation potential parameterized by Wang and Perdew²⁴. Self-consistent field calculations are done with a convergence criterion of 10^{-6} a.u. on the total

energy and electron density. For each cluster size, we started from a number of possible configurations and perform full geometry optimizations with Broyden-Fletcher-Goldfarb-Shanno (BFGS) algorithm. We use convergence criterion of 10^{-3} a.u. on the gradient and displacement, and 10^{-5} a.u. on the total energy in the geometry optimization. For the smaller clusters, different possible spin multiplicities are also tried.

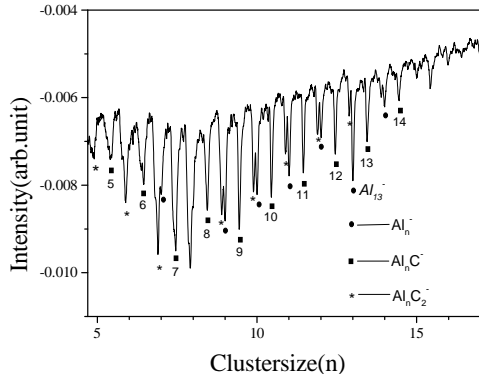


FIG. 1. Mass spectrum for aluminum and aluminum-carbon mixed cluster anions, Al_n^- , Al_nC^- and $Al_nC_2^-$, in the small size range ($n = 5 - 17$). The spectrum peaks for Al_nC^- anions and magic Al_{13}^- clusters are marked. Among the Al_nC^- clusters, a global maximum at Al_7C^- and a less notable local maximum at Al_9C^- can be identified. The detailed spectrum structures around Al_7C^- are further illustrated in Fig.2.

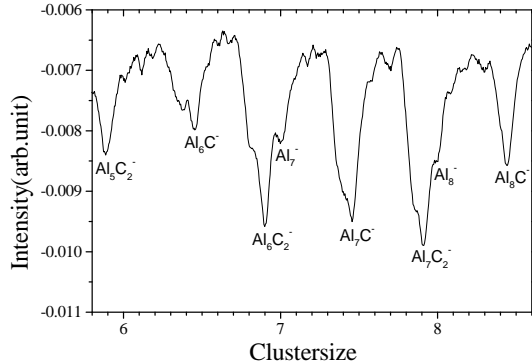


FIG. 2. An expanded spectrum exhibits the more detailed structure of Al_n^- , Al_nC^- and $Al_nC_2^-$ in the mass range from $n = 5$ to $n = 8$.

The spectrum of cluster anions Al_n^- and Al_nC^- in Fig.1 covers the small cluster size ranging from $n = 5$ to $n = 17$. The spectrum is recorded when a helium carrier gas stagnation pressure of 8 atm and a deflection voltage of 90 V exerted on the X-deflector are used. One prominent feature in the spectrum is the well-known magic cluster Al_{13}^- , which corresponds to a complete icosahedral geometrical shell structure⁹ and a $2p$ electronic shell closing with the total number of valence electrons $n_e = 40$ ^{1,2,16}. In Fig.1, three sequential maximum peaks centered at Al_7C^- are also found. For clarity, an

expanded spectrum in the mass region around Al_7C^- with a better resolution is presented in Fig.2. $Al_6C_2^-$, Al_7C^- and $Al_7C_2^-$ are identified as local maxima. It is noted that under the above experimental conditions, these species are always found as local maxima. Therefore, one can conclude from the mass spectrum that the Al_7C^- has the highest abundance among the anionic Al_nC^- clusters. The present results on Al_7C^- agree well with previous experimental mass spectra^{15,21}.

To investigate the aluminum cluster anions in a larger mass range, we use a 10 atm He gas stagnation pressure and a 270 V X-deflection voltage. The spectrum of Al_n^- and Al_nC^- anions recorded in such conditions is presented in Fig.3. In Fig.3, Al_{23}^- is obtained as a local maximum. The seventy valence electrons in Al_{23}^- coincide the $3s$ electronic shell closing under the spherical jellium model^{1,2,16}. The geometric structure of Al_{23}^- may also contribute to its stability^{12,26,27}. Whether the slightly intense Al_{35}^- ($n_e = 106$) peak in the spectrum has an electronic shell origin remains an issue of discussion. Besides, a sudden increase in intensity of Al_{17}^- and $Al_{17}C^-$ is found in Fig.3. Our present mass spectrum of Al_n^- compares well with previous results¹⁵. However, in this study, we would like to pay the particular attention to the unusually stable species Al_7C^- .

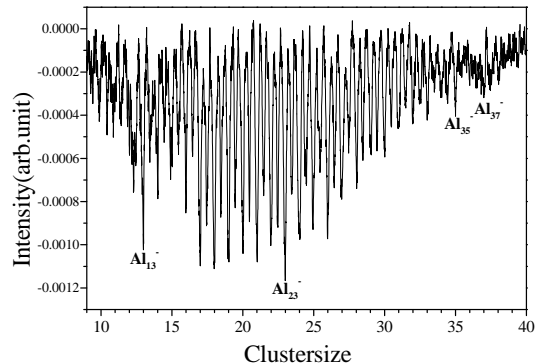


FIG. 3. A mass spectrum of Al_n^- and Al_nC^- in the larger size range.

In this paper, we exploit the lowest energy structures of the Al_nC^- ($n = 1 - 13$) by using density functional geometrical minimization. The obtained ground state structures of Al_nC^- ($n = 1 - 7$, $8 - 13$) are shown in Fig.4 and Fig.5 respectively. In general, the carbon atom is located in the center of the equilibrium structure of Al_nC^- clusters. The calculated cluster properties such as atomization energy and HOMO-LUOM gap are described in Table I. Our present results on the cluster energy difference ΔE_n agree well with previous calculations¹³.

The ground state configurations and bond length parameters of the smaller Al_nC^- ($n = 1 - 4$) compare well with previous calculations in Ref.[13] (Fig.4). Spin triple state is found as ground state of AlC^- and its bond length is 1.89 Å, which agree well with previous calculations^{13,28}. The minimum energy structure found for Al_2C^- is an isosceles triangle (C_{2v}) with bond length

1.85 Å and apex angle $\theta = 110.6^\circ$, in good agreement with the 1.85 Å and 103° obtained from previous *ab initio* calculations¹³. The lowest energy structure of Al_3C^- is a carbon-centered planar triangular structure with C-Al bond length 1.91 Å, which is close to that of 1.90 Å in previous studies^{13,18}. For Al_4C^- , the lowest energy configuration is obtained as a carbon-centered planar trapeziform. The Al-C distances in Al_4C^- are 1.96 and 2.05 Å. This structure is consistent with that in Ref.[13] but different from the symmetric constraint calculation done by L.S.Wang *et al.*¹⁹.

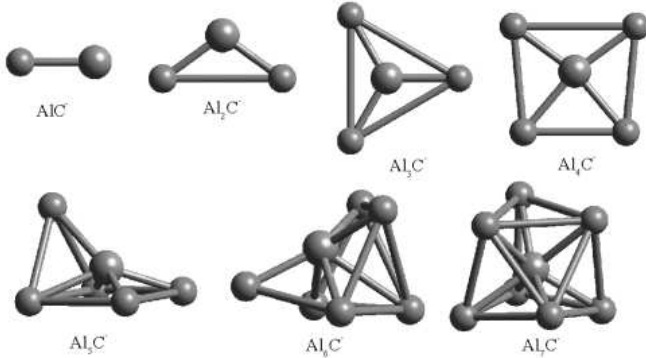


FIG. 4. Lowest-energy structures for small Al_nC^- ($n = 1 - 7$) clusters. The atoms with larger radius denote carbon atom.

Table I. Theoretical atomization energy (AE) and HOMO-LUMO Gap (Δ) for anionic Al_nC^- clusters with $n = 1 - 13$. ΔE_n are the differences in atomization energy between cluster with n and $n - 1$ atoms for Al_nC^- clusters, while ΔE_n^a are those taken from Ref.[13].

Cluster	AE (eV)	ΔE_n (eV)	ΔE_n^a (eV)	Gap (eV)
AlC^-	4.80			0.62
Al_2C^-	9.20	4.40	4.46	2.40
Al_3C^-	13.44	4.24	3.97	2.15
Al_4C^-	15.98	2.54	2.62	1.45
Al_5C^-	18.60	2.62	2.38	0.80
Al_6C^-	21.64	3.04	3.21	0.79
Al_7C^-	25.66	4.02	3.91	1.72
Al_8C^-	27.52	1.86	1.94	0.36
Al_9C^-	30.72	3.20		1.48
Al_{10}C^-	32.95	2.23		0.37
Al_{11}C^-	35.68	2.73		0.87
Al_{12}C^-	39.01	3.33		0.21
Al_{13}C^-	41.46	2.45		0.52

The low-energy structure of Al_5C^- can be considered as being a distorted square pyramid face-capped by one Al atom. This structure has been obtained as a local minimum in previous study²⁰. In our calculation, it is energetically lower than the equilibrium structure (a compressed octahedron) found in Ref.[13] by 0.09 eV. The low-energy structure for Al_6C^- can be constructed by face-capping one more aluminum atom on the configuration of Al_5C^- in Fig.4. However, a carbon-centered triangular prism was found as ground state structure in Ref.[13]. The energy difference between these two isomers is 0.21 eV from our calculation. In the case of Al_7C^- , we find a central carbon surrounded by a seven-atom aluminum cage, in complete agreement with previous work¹³. Thus, the particular low reactivity of Al_7C^- against oxygen²¹ can be partially understood by the close aluminum cage, which can protect the high reactive carbon site from approaching O_2 molecules.

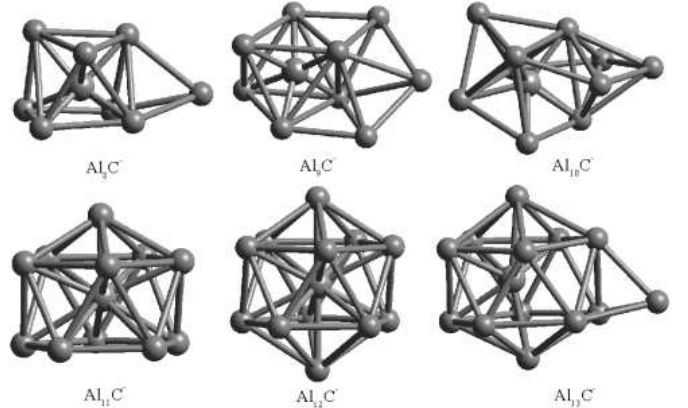


FIG. 5. Lowest-energy structures for larger Al_nC^- ($n = 8 - 13$) clusters. The atoms with larger radius denote carbon atom.

As shown in Fig.5, the low-energy structures of Al_8C^- are based on face-capping of one Al atom on the Al_7C^- cage, which agree with previous calculations¹³. The structure for Al_9C^- can be viewed as a carbon-centered octahedron edge-capped by three atoms. Similar to Al_8C^- , the low-energy structures of Al_{10}C^- can be constructed by face-capping of three aluminum atoms on the cage-like structure of Al_7C^- . Starting from $n = 11$, the equilibrium configurations of Al_nC^- switch to the icosahedron-based packing. Al_{11}C^- is a truncated icosahedron with slight distortion. Al_{12}C^- is a perfect carbon-centered icosahedron with C-Al distance as 2.56 Å. The equilibrium structure of Al_{13}C^- is a distorted carbon-centered icosahedron capped by one Al atom.

In Fig.6, we plot the second differences of cluster energies defined by $\Delta_2 E(n) = AE(n+1) + AE(n-1) - 2AE(n)$, where $AE(n)$ is the atomization energy of Al_nC^- clusters from DFT calculations. In cluster physics, the $\Delta_2 E(n)$ is a sensitive quantity that reflect the stability of clusters and can be directly compared to the experimental relative abundance. In Fig.6, a global

maximum at $n = 7$ and local maxima at $n = 3, 9$ are obtained. The present theoretical results are consistent with our experiment and previous works quite well^{15,21}. In addition to the most pronounced peak at Al_7C^- , our experimental mass spectrum in Fig.1 also show a local maxima at $n = 9$. On the other hand, Al_3C^- was found as a local maximum clusters in Castleman's experiments²¹.

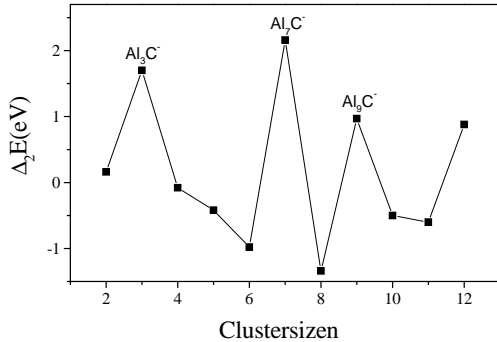


FIG. 6. Second differences of cluster energies $\Delta_2E(n)$ defined as $\Delta_2E(n) = 2AE(n) - AE(n-1) - AE(n+1)$ as a function of cluster size n for $n = 2 - 13$. $E(n)$ is the atomization energy of Al_nC^- clusters. Maxima at $n = 3, 7, 9$ are found.

From our experimental and theoretical investigation, Al_7C^- is always obtained as a magic cluster with pronounced high stability among the anionic Al_nC^- clusters. In addition to the maximum on the size dependent cluster energy difference, ΔE_n or $\Delta_2E(n)$, Al_7C^- also possess a HOMO-LUMO gap of 1.72 eV larger than its neighboring clusters (Table I). Such large gap should have certain contribution to the low reactivity upon oxygen. The particular stability of the Al_7C^- could be useful in construct cluster-based materials. For example, it might be possible to assemble Al_7C^- with alkali metal ions to form stable solid. The further calculations on this direction is still under way and the results will be described elsewhere.

In summary, we have performed both experimental and computational studies on Al_nC^- clusters. Experimental mass spectrum on Al_n^- show the standard magic number at Al_{13}^- and Al_{23}^- due to electron shell closing. Among those anionic Al_nC^- clusters, Al_7C^- is found to be particularly stable. The ground state structures of the Al_nC^- ($n = 1 - 13$) clusters are determined from density functional optimizations. Theoretical calculations also demonstrate the high stability of Al_7C^- , which might be attributed to the stable aluminum cage and large electronic gap. We suggest that the magic Al_7C^- cluster could be building blocks of future cluster-assembled materials.

This work is supported by the U.S. Army Research Office (Grant DAAG55-98-1-0298), NASA Ames Research Center, and the National Natural Science Foundation of China (No.29890210) and National Climbing Project of

China.

* Corresponding author: zhaoj@physics.unc.edu

- ¹ W.A.de Heer, Rev.Mod.Phys.**65**, 611(1993).
- ² M.Brack, Rev.Mod.Phys.**65**, 677(1993).
- ³ *Clusters of Atoms and Molecules I*, Edited by H.Haberland (Springer-Verlag, Berlin, 1994).
- ⁴ *Clusters of Atoms and Molecules II*, Edited by H.Haberland (Springer-Verlag, Berlin, 1994).
- ⁵ G.H.Wang, J.Cluster Sci.**10**, 397(1999).
- ⁶ S.N.Khanna and P.Jena, Phys.Rev.Lett.**69**, 1664(1992).
- ⁷ P.Jena and S.N.Khanna, Mater.Sci.Eng.A**217/218**, 218(1996).
- ⁸ W.Kraschmer, L.D.Lamb, K.Fostiropoulos, D.R.Huffman, Nature **318**, 354(1990).
- ⁹ X.G.Gong, V.Kumar, Phys.Rev.Lett.**70**, 2078(1993).
- ¹⁰ F.Liu, M.Mostoller, T.Kaplan, S.N.Khanna, P.Jena, Chem.Phys.Lett.**248**, 213(1996).
- ¹¹ V.Kumar, V.Sundararajan, Phys.Rev.**B57**, 4939(1998).
- ¹² V.Kumar, S.Bhattcharjee, Y.Kawazoe, Phys.Rev.**B61**, 8541(2000).
- ¹³ C.Ashman, S.N.Khanna, M.R.Pederson, Chem.Phys.Lett.**324**, 137(2000).
- ¹⁴ W.A.Saunders, P.Fayet, L.Woste, Phys.Rev.**A39**, 4400(1989).
- ¹⁵ A.Nakajima, T.Kishi, T.Sugioka, Y.Sone, and K.Kaya, Chem.Phys.Lett.**177**, 297(1991).
- ¹⁶ X.Li, H.Wu, X.B.Wang, L.S.Wang, Phys.Rev.Lett.**81**, 1909(1998).
- ¹⁷ B.C.Liu, H.J.Zhai, R.F.Zhou, G.Q.Ni, Z.Z.Xu, Chin.Phys.Lett.**17**, 658(2000).
- ¹⁸ A.I.Boldyrev, J.Simons, X.Li, W.Chen, L.S.Wang, J.Chem.Phys.**110**, 8980(1999).
- ¹⁹ X.Li, L.S.Wang, A.I.Boldyrev, J.Simons, J.Am.Chem.Soc.**121**, 6033(1999).
- ²⁰ A.I.Boldyrev, J.Simons, X.Li, L.S.Wang, J.Chem.Phys.**111**, 4993(1999).
- ²¹ B.D.Leskiw, A.W.Castleman Jr., Chem.Phys.Lett.**316**, 31(2000).
- ²² G.Q.Ni, R.F.Zhou, H.J.Zhai, Y.Z.Wang, Chin.Phys.Lett.**14**, 633(1997).
- ²³ DMOL is a density functional theory (DFT) package based atomic basis distributed by MSI. B.Delley, J.Chem.Phys.**92**, 508(1990).
- ²⁴ Y.Wang and J.P.Perdew, Phys.Rev.**B43**, 8911(1991).
- ²⁵ M.Y.Zhou and M.L.Cohen, Phys.Lett.**A113**, 420(1986).
- ²⁶ T.P.Martin, T.Bergmann, H.Gohlich, T.Lange, J.Phys.Chem.**95**, 6421(1991).
- ²⁷ E.K.Parks, B.J.Winter, T.D.Klots, S.J.Riley, J.Chem.Phys.**94**, 1882(1991).
- ²⁸ G.L.Gutsev, P.Jena, R.J.Burtlett, J.Chem.Phys.**110**, 2928(1999).